DFT insights into Mechanical and Anisotropic Properties of $AZnF_3$ (A = Li, K, and Rb) Systems under Pressure

Abderrahim Hadj Larbi*[1], Moufdi Hadjab[2], Abderrazak Hamam[1], Ala Boulegane[1], Fayçal Bouzid[1], Radhia Yekhlef[1]

[1]Research Center in Industrial Technologies CRTI, P.O. Box 64, Cheraga 16014, Algiers, Algeria

[2]Department of Electronics, Faculty of Technology, University of M'sila, Algeria

***Corresponding author: hadjlarbi@gmail.com**

Received 11 September 2023, Accepted 15 November 2023, Published 10 December 2023

Abstract

The study predicts the electronic, mechanical and anisotropic properties of AZnF3 perovskite compounds, where A represents Li, K, and Rb. Ground state functions are computed using the full potential linearized augmented plane wave (FP-LAPW) method. A close agreement is observed when comparing the calculated ground state structural parameters with available results. The elastic constants induced by pressure reveal the mechanical stability of the studied materials, satisfying the Born stability criteria. Regarding Young's modulus, shear modulus, and Poisson's ratio, RbZnF3 stands out as the compound exhibiting ductile behavior. LiZnF3 displays the highest shear stiffness and possesses the greatest resistance to deformation when compared to the other fluoroperovskites investigated in this study. With increasing pressure, these fluoroperovskites become more and more ductile at higher pressure. The discussion delves into the elastic moduli's dependence on pressure, emphasizing the overall anisotropic nature of the studied compounds.

Keywords: Halide perovskites, first-principles study, DFT, elastic property, anisotropy

*Tob Regul Sci.™ 2023;9(2):*3019 - 3037

DOI: doi.org/10.18001/TRS.9.2.195

1. Introduction

In the past decade, halide perovskites (ABX_3) have emerged as compelling materials for next-generation high-performance solar cells, photodetectors, and lasers, among other applications[1–9]. Halide perovskites have gained considerable attention, thanks to their different physicalproperties[10,11]. Some of these properties arise from the perovskite structure and the variety of elements they may include, featuring a monovalent organic or inorganic A^{1+} cation, a divalent metal B^{2+} cation, and a halide X^{1-} anion, such as F^{1-}, Cl^{1-}, Br^{1-}, or I^{1-}.The wide applications, and the limited available information on the properties of halide perovskites, specifically Zn-based fluoroperovskite motivate us to investigate these compounds here.

Idrissi et al investigateddifferent optical properties of $AgZnF_3$ $LiZnF_3$ and $NaZnF_3$[12]. Kumari et al studied physical features of $RbXF_3$[13].Theoretical work has been done by Erum et al on series of cubic perovskites $RbMF_3$[14]. Shakeel et al investigated anisotropic and physical properties of XYF_3[15].Eventually, Mouna et al worked on the influence of pressure on physical properties of $KBeF_3$, $RbBeF_3$ compounds [16].

For $AZnF_3$ (A = Li, K, Rb) structures, several studies have focused on the electronic and optical properties. Nevertheless, there is insufficient literature on the impact of pressure on the mechanical properties and anisotropy insights of these compounds. Furthermore, the mechanical properties and pressure-induced behaviors are still unexplored. It is worth noting that in the case of $LiZnF_3$, both Li and Zn ions are of comparable size, yet the fluoroperovskite structure is possible and has been reported in the Inorganic Crystal Structure Database (ICDD)[17]. To address this knowledge gap, The objective of this research is to enhance our understanding of the electronic, mechanical, and anisotropic properties of $AZnF_3$ (A = Li, K, and Rb) under pressure. This studybased on theoretical analysisby employing the density functional theory (DFT) with generalized gradient approximation (GGA) embodied in Wien2k code[18]. The remainder of this paper is structured as follows: The proposed computational technique is described in Section 2, and findings regarding the structural, electronic, and mechanicalproperties of $AZnF_3$ (A = Li, K, and Rb) compounds are analyzed in Section 3. Section 4 reviews the major conclusions of this research.

2.Computational details

In this investigation, we conducted comprehensive calculations using the FP-LAPW method, a density functional theory (DFT) approach implemented in the Wien2k package[18–20].Initially, we applied the generalized gradient approximation (GGA)to optimize crystal structures and determine electronic bands[21]. The separation of valence and core states employed a plane wave cut-off energy of -6 Ryd, with a matrix size defined as Rmt × Kmax = 9, where Kmax signifies the plane wave cut-off and Rmt is the minimum atomic sphere radius. Distinct atomic sphere radii were assigned for Li, K, Rb, Zn, and F, namely 2.5, 2.5, 2.5, 1.8, and 1.7 atomic units, respectively. The maximum number of partial waves within the muffin-tin spheres was expanded up to lmax = 10. The Monkhorst-Pack method facilitated k-integration over the Brillouin zone using a 10 × 10 × 10 k mesh in the irreducible wedge[22]. Convergence in the self-consistent calculation was determined when the total energy difference fell below 0.0001 Ryd. Electronic configurations for chemical atoms were specified as follows: Li ($1s^2$ $2s^1$), K ($3s^23p^64s^1$), Rb ($4s^24p^65s^1$), Zn ($1s^22s^22p^63s^23p^63d^{10}4s^2$), and F ($1s^22s^22p^5$).

3.Results and discussion

3.1. Structural stability and energy gap

The Fluoroperovskites have a cubic structure with the highest symmetry space group of Pm-3m at room temperature[23]. In the case of $AZnF_3$ (where A = Li, K, or Rb) as shown in Fig.1, the cations (Li, K, or Rb) occupy the (0, 0, 0) position in a cuboctahedral site. Zinc is located at the center of the cube at (0.5, 0.5, 0.5) in an octahedral site, while the fluoride anions are positioned at the centers of the cube's faces with coordinates (0.0, 0.5, 0.5), (0.5, 0.0, 0.5), and (0.5, 0.5, 0.0).

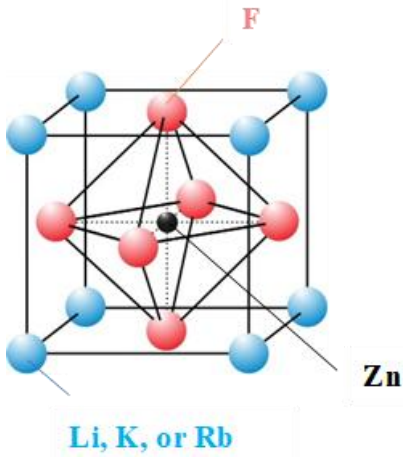

Fig. 1. Crystal structure of the cubic perovskite $AZnF_3$ (A=Li, K, or Rb)

Table 1. Calculated lattice parameter a (Å), and Bulk modulus B (GPa) of $AZnF_3$ (A = Li, K and Rb), using GGA–PBESol, compared to some experimental and other theoretical works.

	a_0	K	Ref.
$LiZnF_3$	3.97	82.94	This work
	-	-	Experimental
	3.96 [12]	-	Other work
$KZnF_3$	4.06	79.19	This work
	4.05 [24]	77.6 [25]	Experimental
	4.06 [26]	77.21 [26]	Other work
$RbZnF_3$	4.11	79.33	This work

	4.12 [27]	-	Experimental
	4.11 [15]	79.34 [15]	Other work

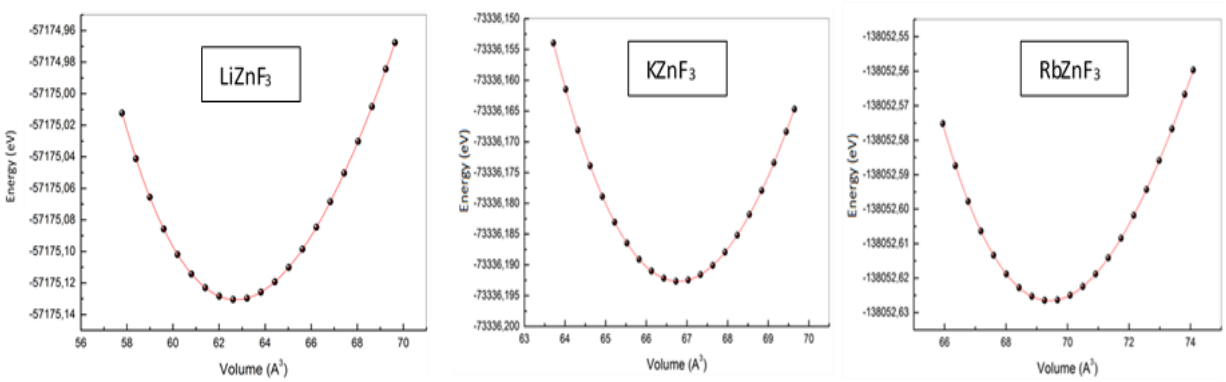

Fig. 2. Total energy of $AZnF_3$ (A = Li, K and Rb) as a function of volume (Å), using GGA–PBESol

Analyzing the structural properties is crucial for predicting various physical properties through ab initio methods. Many previous studies have extensively tested and established the well-known efficacy of the PBEsol functional in predicting the structural properties of solid materials [28,29]. This is accomplished by systematically varying the unit cell volume in the studied compounds and aligning it with the well-established Murnaghan equation[30]. The goal is to determine the optimal values of the lattice parameter 'a' (in Å). Therefore, this approach enables us to determine various structural parameters, such as the lattice parameter, bulk modulus, which are presented in table 1 and compared to both experimental and other theoretical findings.Our results align well with both existing theoretical and experimental values. Fig. 2 illustrates the variation of the unit cell volume as a function of energy for the examined compounds ($LiZnF_3$, $KZnF_3$, and $RbZnF_3$). The continuous line represents the Murnaghan fit applied to our calculated data points.

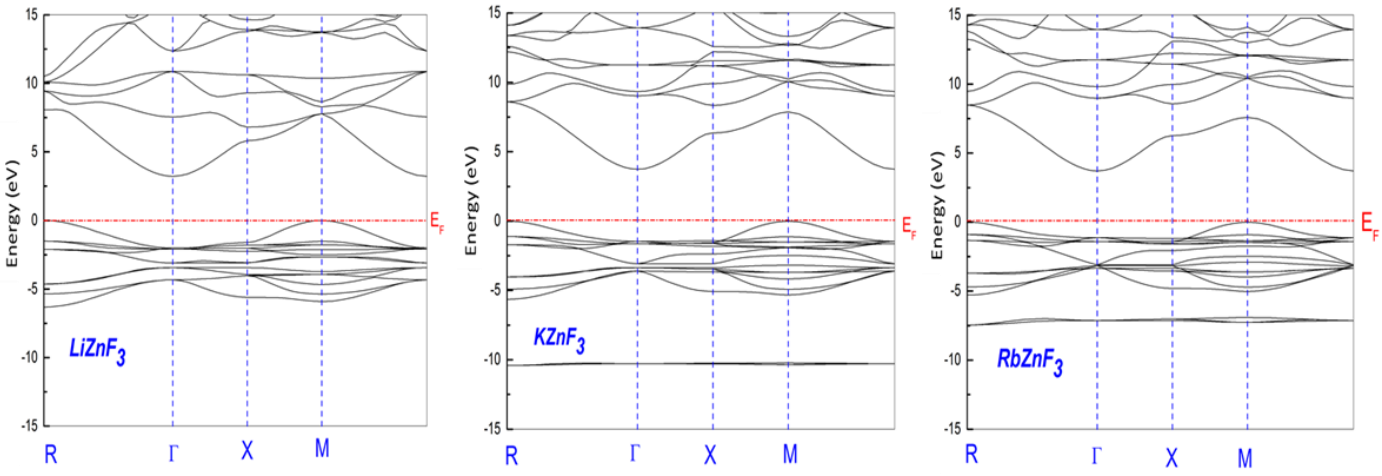

Fig. 3. Band structures of $AZnF_3$ (A= Li, K, and Rb)at 0 GPa, using the GGA-PBE approximation

To describe the trend of the energy gap as a function of hydrostatic pressure, we calculated the gap energy of $AZnF_3$ (A= Li, K, and Rb) at different pressures ranging from 0 to 10 gigapascals (GPa). At 0 GPa, we plotted the band structure of the three compounds in Fig. 3. The figure illustrates that all these unpressed compounds exhibit an indirect band gap between the valence band maximum at the R symmetry point and the conduction band minimum at the Γ symmetry. The calculated band gaps at zero pressure, using the GGA approximation, are 3.23 eV for $LiZnF_3$, 3.73 eV for $KZnF_3$, and 3.70 eV for $RbZnF_3$. The changes in the band gap values of these compounds are calculated under hydrostatic pressure and plotted in Fig. 4. For $LiZnF_3$ the band gap slightly decreases through the pressure variation, but for $KZnF_3$ and $RbZnF_3$, the band gap increases as the pressure increases in the range 0–10 GPa.

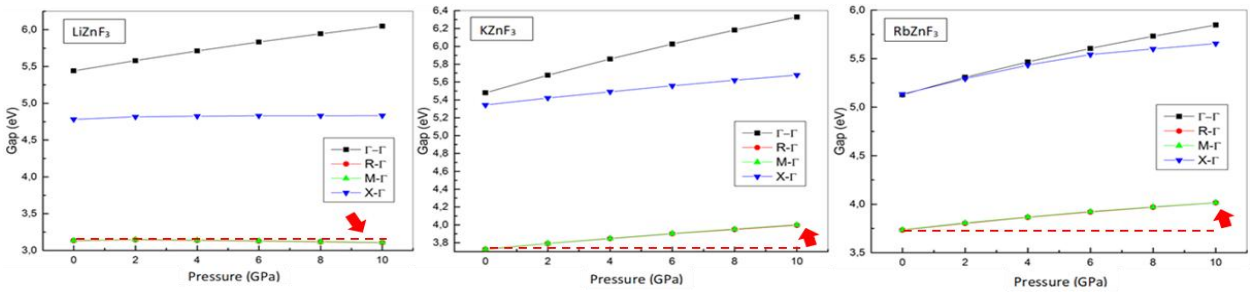

Fig. 4. Variation of band gap (R-Γ) and energy difference of high symmetry points (Γ-Γ, X-Γ, M-Γ) in the function of the pressure up to 10 GPa for $AZnF_3$ (A = Li, K, and Rb) compounds.

We can explain the decrease of gap energy of $LiZnF_3$, by the impact of pressure on the volume. This impact is inevitably a direct result of volume contraction which rise the overlap between the neighboring orbitals which is responsible for the increase in the electronic band dispersion. These bands comprise of antibonding, bonding and nonbonding orbitals. By applying pressure, the overlap between these orbitals increases, the antibonding nature of the bands pushing it up while the bonding nature dropping it down and thus the bands dispersed. In this way, it is very clear that when the conduction and valence bands spread the band gap energy decreases.

The increase in the band gap for $KZnF_3$ and $RbZnF_3$can be interpreted on the basis of the nature of bonding(covalent and ionic) in these compounds. The main contribution in the band gap opening to the pressure dependence arises from the covalent energy [31]. With pressure, the covalent nature increase in these compounds which cause greater covalent energy and result in the band gap opening[15]. This effect is predominantly due to nonbonding and antibonding nature of bands closer to the Fermi level, which are specifically responsive to pressure.

3.2. Elastic constants and mechanical properties

The usual starting point of elastic theory is the Hooke's law, which states that stress is proportional to strain for small deformations. An elastic crystal spontaneously returns to its original shape when external stresses are removed. Therefore, the deformation always remains in the vicinity of a natural state of the system, which is an equilibrium state where all stresses cancel out.

The following relation defines Hooke's law.

$$\sigma_{ij} = \sum_{kl} C_{ijkl}\varepsilon_{kl}\,. \tag{1}$$

Where $\sigma_{ij}$is the stress tensor, $\varepsilon_{kl}$is the strain tensor, and $C_{ijkl}$are the elastic constants.

The basic understanding of how stress-free crystalline structures remain mechanically stable has been established since the research conducted by Born[32]. Subsequent studies have outlined the general requirements for elastic stability in crystal lattices and have provided simplified conditions for specific types of highly symmetrical crystals. Specifically, for cubic crystals, the stability conditions can be expressed in a straightforward manner[33]:

$$C_{11} - C_{12} > 0, \qquad C_{11} + 2C_{12} > 0, \qquad C_{44} > 0. \tag{2}$$

These conditions are necessary and sufficient to determine the mechanical stability of these stress-free materials.However, when subjected to isotropic compression, cubic crystals exhibit three other distinct stability conditions [34–36]:

$$M_1 = (C_{11} + 2C_{12} + P)/3 > 0,$$

$$M_2 = C_{44} - P > 0, \tag{3}$$

$M_2 = (C_{11} + C_{12})/2 - P > 0.$

From the elastic constant data, the bulk modulus K and shear modulus G can generally be calculated using the Voigt approximation[37]and the Reuss approximation methods [38].

For a cubic crystal, the Voigt bulk modulus (K_V), and Reuss bulk modulus (K_R) are given by following relationships[39,40]:

$$K_V = K_R = \frac{1}{3}(C_{11} + 2C_{12}). \tag{4}$$

And Voigt shear modulus (G_V) and Reuss shear modulus (G_R) are defined as[39]:

$$G_V = \frac{1}{5}(C_{11} - C_{12} + 3C_{44}), \tag{5}$$

$$G_R = \frac{5\,C_{44}(C_{11} - C_{12})}{4C_{44} + 3\,(C_{11} - C_{12})}. \tag{6}$$

Hill proposed that the bulk modulus (K) and shear modulus (G) be the arithmetic averages of the Voigt and Reuss bulk and shear moduli[39]:

$$K = \frac{1}{2}(K_V + K_R\ ),\ \ G = \frac{1}{2}(G_V + G_R). \tag{7}$$

Furthermore, the Young's modulus E and Poisson's ratio ν can be given by[39]:

$$E = \frac{9KG}{3K + G}, \tag{8}$$

$$\nu = \frac{3K - 2G}{6K + 2G}. \tag{9}$$

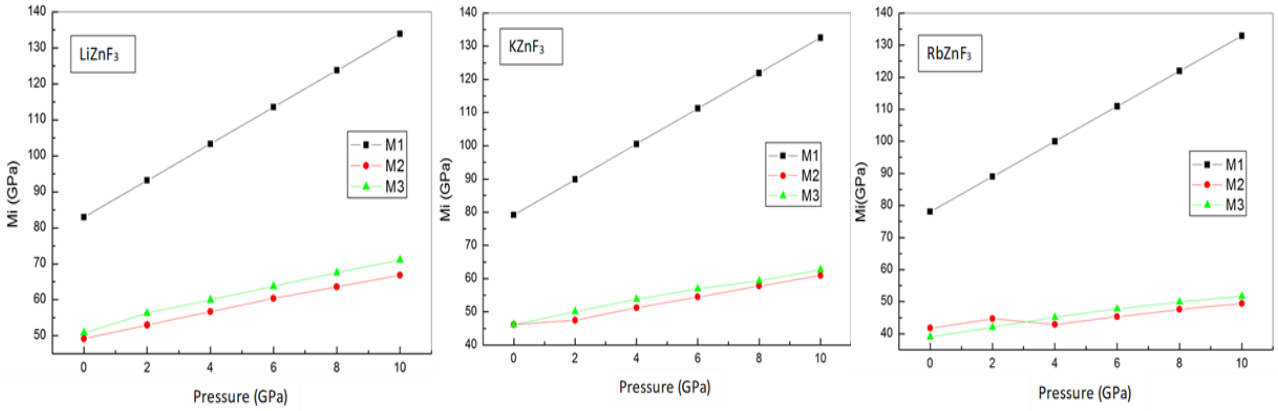

Fig. 5. Variation of generalized stability criteria M_i in function of pressure for $AZnF_3$ (A=Li, K, and Rb) materials

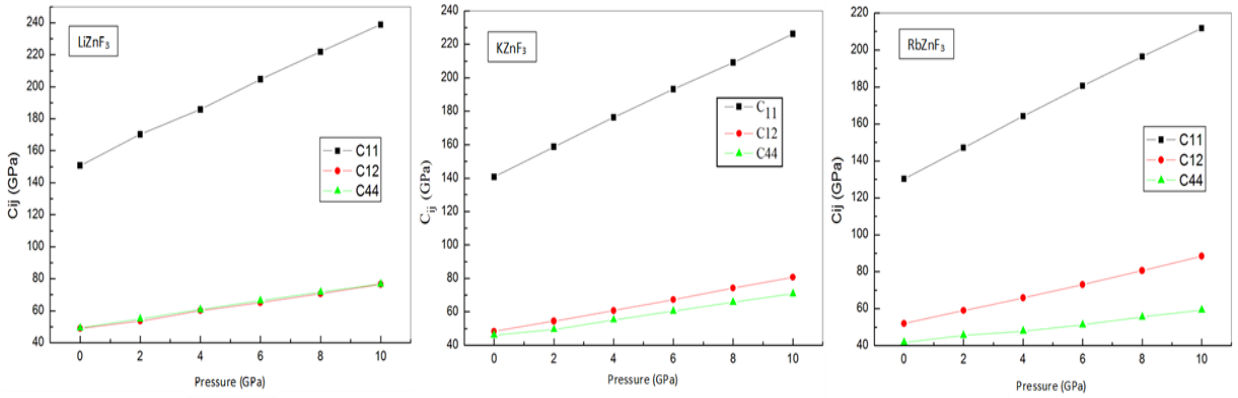

Fig. 6. Variation of elastic constants C_{ij} in function of pressure for $AZnF_3$ (A=Li, K, and Rb) materials

By applying hydrostatic pressure (P) in the range of 0 GPa to 10 GPa, we obtained the M_i and C_{ij} values as illustrated in Fig. 5 and Fig.6. The stability criteria as demonstrated in Fig.5, reveal that all values of M_i are positive for the three materials. Fig.6 depictsthe pressure-dependent behavior of elastic constants,showcasing a significant increase in C_{ij} with rising pressure. Notably, the elastic constants C_{ij} exhibit a linear increase with the rise in pressure, thereby supporting the generalized stability criteria of the $AZnF_3$ (A = Li, K, and Rb) materials. Furthermore, Aguado et al experimentally confirmed the stability of $KZnF_3$ perovskite structure in the explored range [41]. Consequently, this information provides valuable insights into the anticipated physical properties of these compounds within the specified pressure range.

Notably, the generalized gradient approximation (GGA) consistently overestimates C_{11}, C_{12}, and C_{44}[42]. The elastic constants depend sensitively on the volume, and therefore, an error depending on the error in volume is introduced in the calculated elastic constants compared to experimental volume. It is imperative to exercise caution, recognizing that the calculated values are specific to 0 K, whereas experimental investigations are conducted at room temperature. Generally, an elevation in temperature tends to diminish elastic constants due to thermal expansion [23].

Table 2. Calculated single-crystal elastic constants (Cij in GPa) and polycrystalline elastic moduli (K, G, E in GPa) along with Pugh's ratio (K/G), Poisson's ratio (ν), Anisotropy (A) for $AZnF_3$ (A = Li, K, Rb) materials at 0 GPa and 10 GPa.

		C_{11}	C_{12}	C_{44}	K	G	E	K/G	ν	A	Ref.
$LiZnF_3$	0 GPa	150.67	49.07	49.17	82.94	49.82	124.53	1.66	0.249	0.97	This work
	10 GPa	239.21	77.15	77.12	131.17	78.65	196.65	1.67	0.250	0.95	This work
	0 GPa	-	-	-	-	-	-	-	-	-	Experimental
$KZnF_3$	0 GPa	140.44	48.54	45.88	79.17	45.91	115.42	1.72	0.257	0.998	This work
	10 GPa	226.12	80.85	69.97	129.27	71.02	180.09	1.82	0.267	0.963	This work
	0 GPa	134.4	53.2	38.3	-	-	-	-	-	-	[23]^{Experiment}
	0 GPa	137.93	46.86	42,77	-	43.88	110.66	1.76	0.261	0.939	[26]^{GGA}
$RbZnF_3$	0 GPa	130.24	51.96	41.81	78.05	40.72	104.06	1.92	0.277	1.068	This work
	10 GPa	211.53	89.49	50.98	130.17	54.78	144.13	2.37	0.315	0.835	This work

0 GPa	-	-	-	-	-	-	-	-	-	Experimental
0 GPa	113.81	47.16	35.76	69.37	34.79	89.36	1.99	0.285	1.07	[43]^{GGA}

The elastic constants C_{11}, C_{12}, and C_{44} play distinct roles in characterizing material properties, where C_{11} signifies the elasticity in length, while C_{12} and C_{44} quantify elasticity in shape while maintaining a constant volume. In Fig. 6, its evident that both C_{12} and C_{44} exhibit lower sensitivity to pressure compared to C_{11}. It is noteworthy that C11 consistently surpasses C_{44} for all compounds, suggesting that these materials generally offer less resistance to shear stress compared to their resistance against unidirectional compression. In addition, LiZnF3 stands out with the highest value of C_{11} among all systems, indicating its exceptional incompressibility under uniaxial stress along the a-axis. For more details, Table 2 presents an overview of the specific elastic constants and elastic moduli of polycrystalline materials, along with their corresponding mechanical parameters, for $AZnF_3$ (A= Li, K, and Rb) under a pressure of 0 GPa and 10 GPa.

Examination of these data reveals that $LiZnF_3$ exhibits the highest bulk modulus (K), followed by $KZnF_3$, and $RbZnF_3$. In general, the capacity of a substance to withstand volumetric deformation when subjected to hydrostatic compression can be effectively assessed using the bulk modulus (K). These findings suggest that $LiZnF_3$ possesses the least compressibility among the examined compounds.Similarly, the observed trends in the shear modulus (G) and Young's modulus (E) show that $LiZnF_3$ demonstrating the highest values, followed by $KZnF_3$ and $RbZnF_3$. Shear modulus (G) serves as a measure of its resistance to deformation under shear stress, and Young's modulus (E) denotes the degree of rigidity (resistance to axial loading). This indicates that $LiZnF_3$ displays the highest shear stiffness and possesses the greatest resistance to deformationwhen compared to the other fluoroperovskites investigated in this study.

In light of these findings, and at 0 GPa, we found that the K/G ratio for $RbZnF_3$ exceeds Pugh's critical threshold of 1.75, which is a widely utilized empirical relationship for predicting the brittle/ductile behavior of solids[44]. When the K/G ratio surpasses 1.75, a material exhibits ductile behavior, while values below this threshold indicate brittle behavior. Consequently, based on our calculation, we can categorize $RbZnF_3$ as a ductile material. Conversely, the K/G ratio for LiZnF3 falls below 1.75, while the KZnF3 ratio slightly dips below 1.75, indicating that this compound can be characterized as a brittle material. Brittle materials lack the ability to withstand significant thermal shocks due to their limited capacity to dissipate thermal stress through plastic deformation, resulting in a rapid decline in their mechanical properties at elevated temperatures.

With increasing pressure, this ratio increases, as seen in table 2, which exhibits that these fluoroperovskites become more and more ductile at higher pressure.

Poisson's ratio (ν) is another quantity, that defines the ratio between transverse strain and longitudinal strain in the elastic loading direction therefore provides insight into the way the structural elements are packed,the nature of bonding in solids, and the directions of bonding forces[45,46]. Frantsevich et al. proposed that materials exhibit ductile behavior when the Poisson's ratio exceeds 0.26, otherwise, they are deemed brittle[47]. The computed Poisson's ratio values for $RbZnF_3$, as presented in Table 2, surpass 0.26, unequivocally indicating the ductile nature of the studied materials. The table further demonstrates an increase in Poisson's ratio with pressure, consequently, pressure increasing ductility for $AZnF_3$(A=Li, K, and Rb) perovskites at high pressure. Additionally, Covalent crystals typically have a Poisson's ratio of ~0.10, while that for ionic crystals is approximately ~0.25 [48]. Therefore, based on the ν values (cf. Table 2), the current fluoroperovskites are anticipated to fall into the category of ionic materials. Furthermore, bonding forces between atoms are considered central when ν falls within the range of 0.25–0.50[49]. The results of this study indicate that, for $AZnF_3$ (A = Li, K, Rb) materials, inter-atomic forces are predominantly central.

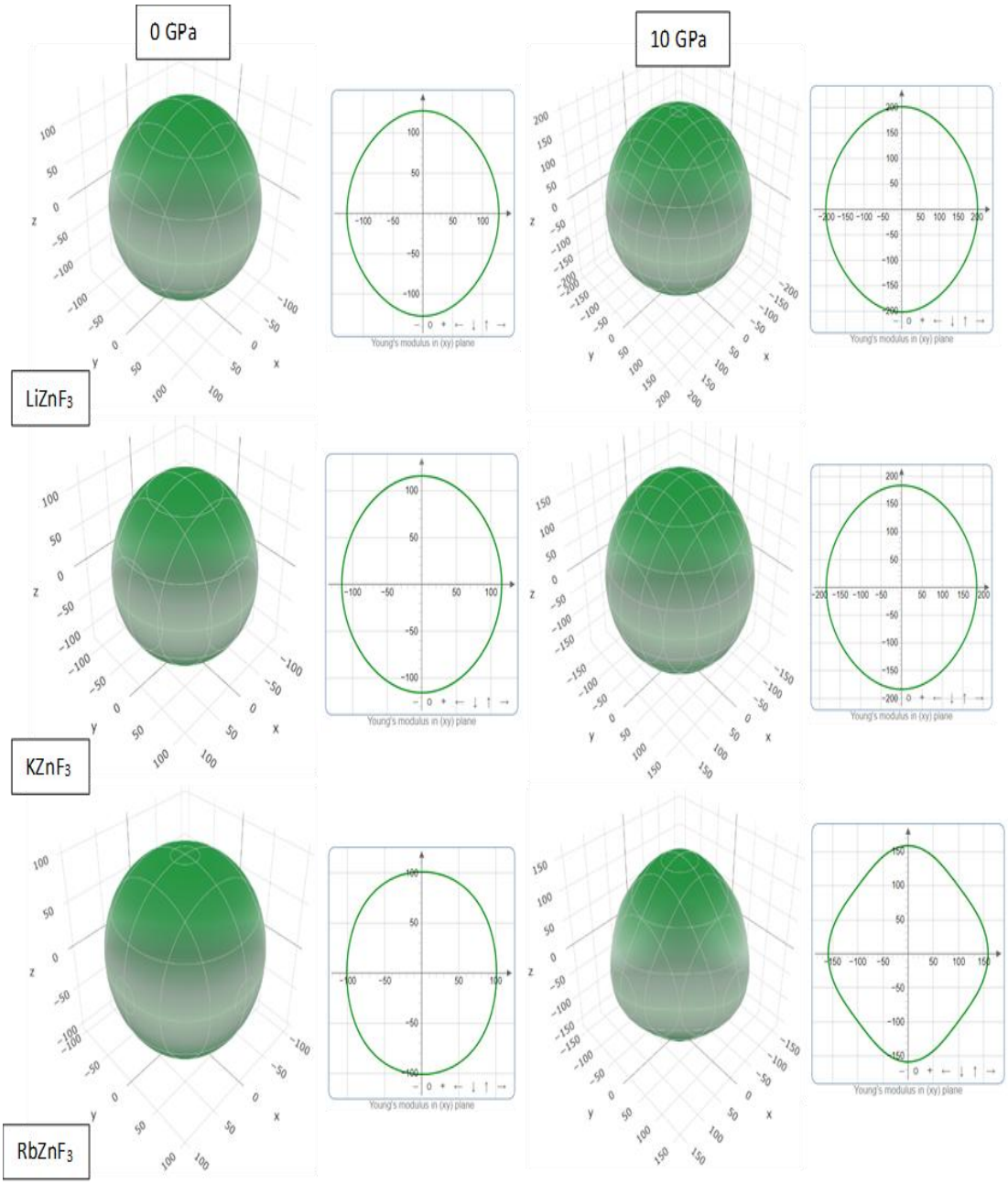

Fig. 7. 2D and 3D Visualization of spatial dependence of Young's modulus (E) of $AZnF_3$ (A=Li, K, and Rb) materials

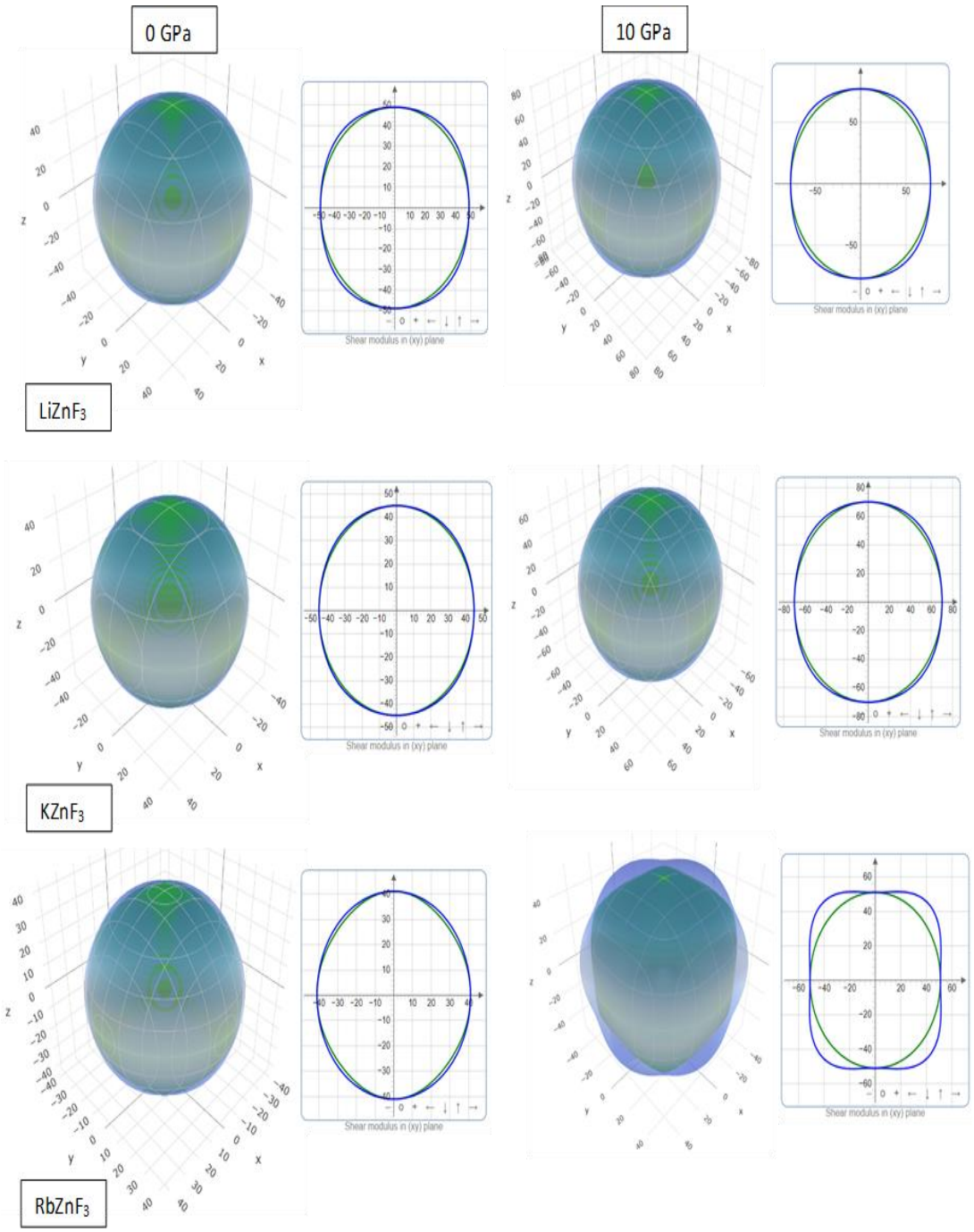

Fig. 8. 2D and 3D Visualization of spatial dependence of Shear modulus (G) of $AZnF_3$ (A=Li, K, and Rb) materials

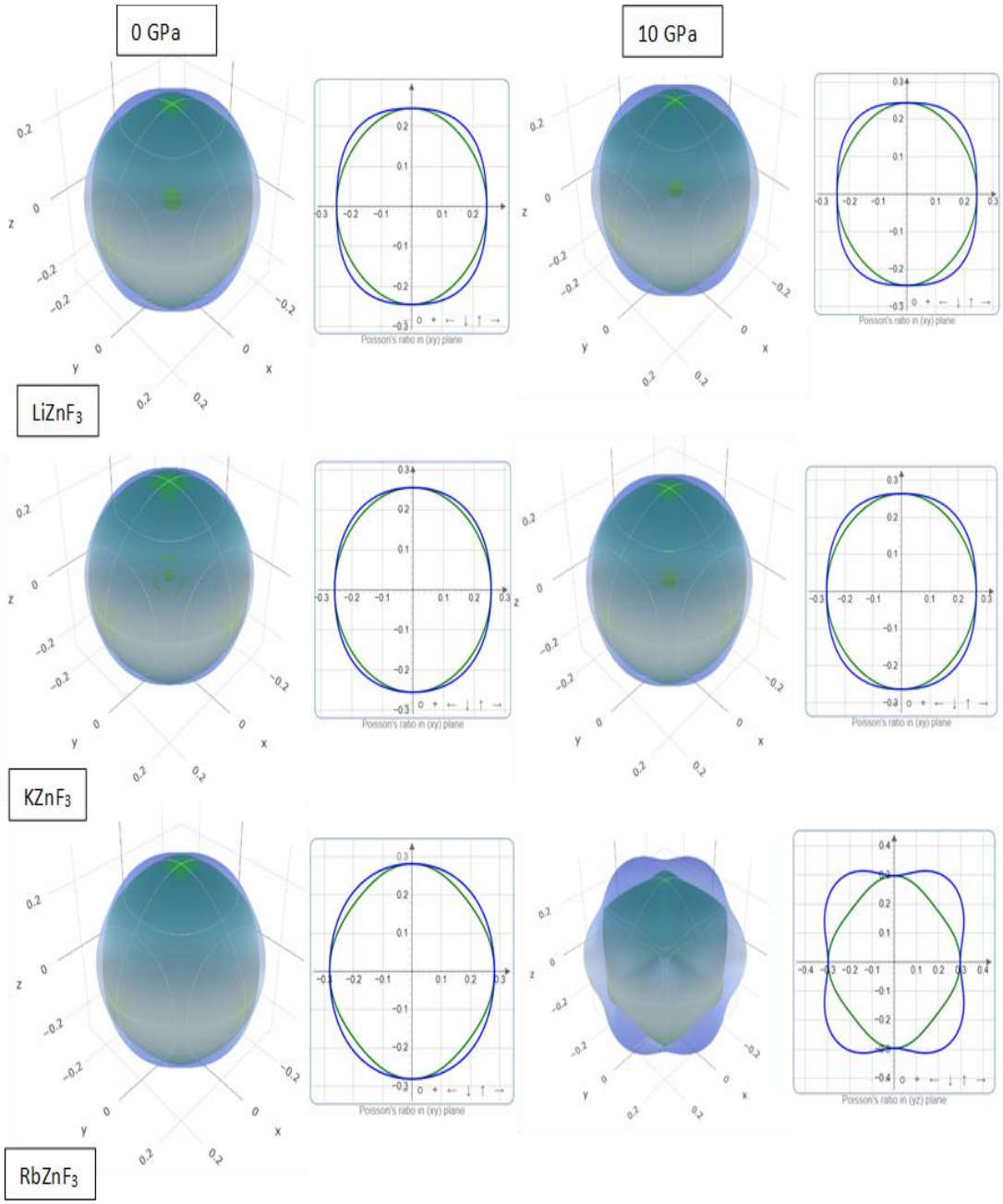

Fig. 9. 2D and 3D Visualization of spatial dependence of Poisson's ratio (ν) of $AZnF_3$ (A=Li, K, and Rb) materials

In the end, solids possess various practical applications due to their knowledge of anisotropic behavior. Anisotropic behavior is applied to evaluate a lot of physical processes, including plastic behavior, phase transition, and the formation of micro-fractures within the materials. Mechanical anisotropy can be assessed using anisotropy indices and 3D graphical representations of elastic moduli. To investigate the elastic anisotropy of crystals based on their moduli, we utilized the ELATE program to generate three-dimensional (3D) contour graphs, and their projections along (xy) planes[50]. Fig. 7-9 depict elastic moduli such as Young's modulus (E), shear modulus (G),

and Poisson's ratio (ν) for fluoroperovskites $AZnF_3$ (A = Li, Zn, and Rb) at pressures of 0 GPa, and 10 GPa. The data for these plots were obtained from calculated C_{ij}. The degree of anisotropy in solids can be discerned through these (3D) plots, where perfect isotropy is represented by a spherical shape, and any deviation from this sphere indicates the extent of anisotropy; where the maximum and minimum values are indicated through blue and green color.

The anisotropy in Young's modulus, shown in Fig.7, does not exhibitclearly in $LiZnF_3$, $KZnF_3$, and$RbZnF_3$. However, the pressure increases the level of anisotropy for $RbZnF_3$, unlike the other materials of $LiZnF_3$ and $KZnF_3$.At 10 GPa and for $RbZnF_3$, the maximum value of Young's modulus appears along the <100> direction and the minimum value occurs along the <110> direction. The shear modulus exhibits a maximum value along the <110> direction and a minimum value along the <100> directions for the three compounds, but appear more clearly for $RbZnF_3$. The maximum value of Poisson's ratio appears along the <110> and the minimum value appears along the <100> direction.Through the whole elastic anisotropy feature analysis of $AZnF_3$ (where A = Li, K, and Rb) we have obtained that Poisson's ratio exhibits highest anisotropic manner compared to other elastic parameters. Comparative the 3D plots and the anisotropy values in Table 2 reveals that the sequence of anisotropy is$RbZnF_3$ > $LiZnF_3$ > $KZnF_3$.

4. Conclusion

In this work, we have studied the pressure effects on band gaps, and mechanical properties of $AZnF_3$ (A = Li, K, and Rb), applying the FP-LAPW method in the framework of DFT. Our results agree well with the experimental data, and other theoretical calculations. The structural stability, mechanical,and anisotropic properties of $AZnF_3$ (Ae = Ca, Sr, Ba) halide perovskite have been carried out successfully employing the first-principles method based on the DFT within GGA. A fair agreement has been found while comparing the calculated ground state parameters with available results, validated the herein method used. The pressure induced elastic stability was further assessed by Born stability criteria and found all materials as elastically stable under considered pressure up to 10GPa. Based on the calculated elastic moduli, various mechanical properties under pressure are evaluated; among them,Young's modulus, shear modulus, and Poisson's ratio predicted that $RbZnF_3$ compound behave as ductile, while LiZnF3 exhibits the highest shear stiffness and possesses the greatest resistance to deformation when compared to the other compounds investigated in this study. All anisotropy factors regarding elastic moduli indicate that the studied fluoroperovskites are elastically anisotropic.

References

[1] Yang W S, Park B-W, Jung E H, Jeon N J, Kim Y C, Lee D U, Shin S S, Seo J, Kim E K, Noh J H and Seok S I 2017 Iodide management in formamidinium-lead-halide–based perovskite layers for efficient solar cells *Science*356 1376–9

[2] Kojima A, Teshima K, Shirai Y and Miyasaka T 2009 Organometal Halide Perovskites as Visible-Light Sensitizers for Photovoltaic Cells *J. Am. Chem. Soc.***131** 6050–1

[3] Jiang T and Fu W 2018 Improved performance and stability of perovskite solar cells with bilayer electron-transporting layers *RSC Adv.***8** 5897–901

[4] Zhou W, Zhou P, Lei X, Fang Z, Zhang M, Liu Q, Chen T, Zeng H, Ding L, Zhu J, Dai S and Yang S 2018 Phase Engineering of Perovskite Materials for High-Efficiency Solar Cells: Rapid Conversion of CH3NH3PbI3 to Phase-Pure CH3NH3PbCl3 via Hydrochloric Acid Vapor Annealing Post-Treatment *ACS Appl. Mater. Interfaces***10** 1897–908

[5] Dou L, Yang Y (Micheal), You J, Hong Z, Chang W-H, Li G and Yang Y 2014 Solution-processed hybrid perovskite photodetectors with high detectivity *Nat Commun***5** 5404

[6] Hu X, Zhang X, Liang L, Bao J, Li S, Yang W and Xie Y 2014 High-Performance Flexible Broadband Photodetector Based on Organolead Halide Perovskite *Advanced Functional Materials***24** 7373–80

[7] Fang Y, Dong Q, Shao Y, Yuan Y and Huang J 2015 Highly narrowband perovskite single-crystal photodetectors enabled by surface-charge recombination *Nature Photon***9** 679–86

[8] He X, Liu P, Wu S, Liao Q, Yao J and Fu H 2017 Multi-color perovskite nanowire lasers through kinetically controlled solution growth followed by gas-phase halide exchange *J. Mater. Chem. C***5** 12707–13

[9] Cha H, Bae S, Jung H, Ko M J and Jeon H 2017 Single-Mode Distributed Feedback Laser Operation in Solution-Processed Halide Perovskite Alloy System *Advanced Optical Materials***5** 1700545

[10] Wangyang P, Gong C, Rao G, Hu K, Wang X, Yan C, Dai L, Wu C and Xiong J 2018 Recent Advances in Halide Perovskite Photodetectors Based on Different Dimensional Materials *Advanced Optical Materials***6** 1701302

[11] Green M A, Ho-Baillie A and Snaith H J 2014 The emergence of perovskite solar cells *Nature Photon***8** 506–14

[12] Idrissi S, Mounkachi O, Bahmad L and Benyoussef A 2023 Study of the solar perovskites: XZnF3 (X = Ag, Li or Na) by DFT and TDDFT methods *J. Korean Ceram. Soc.***60** 424–33

[13] Kumari M, Abraham J A, Sharma R and Datar S 2023 Insights into structural, elastic, mechanical, opto-electronic, and thermoelectric properties of rubidium-based

fluoroperovskites RbXF3 (X = Zn, Cd, Hg) *Journal of Physics and Chemistry of Solids***178** 111357

[14] Erum N and Ahmad J 2023 Structural, Elastic and Mechanical Properties of Cubic Perovskite Materials *Archives of Advanced Engineering Science* 1–9

[15] Shakeel, Reshak A H, Khan S, Laref A, Murtaza G and Bila J 2020 Pressure induced physical variations in the lead free fluoropervoskites XYF3 (X=K, Rb, Ag; Y=Zn, Sr, Mg): Optical materials *Optical Materials***109** 110325

[16] Mouna S C, Radjai M, Rahman Md A, Bouhemadou A, Abdullah, Houatis D, Allali D, Essaoud S S and Allaf H 2024 Physical properties of Be-based fluoroperovskite compounds $XBeF_3$ (X = K, Rb): a first-principles study *J. Phys.: Condens. Matter***36** 055701

[17] Jog M, Patil R R, More Y, Kumar M, Kulkarni M S and Moharil S V 2018 PHOTOLUMINESCENCE, THERMOLUMINESCENCE AND OPTICALLY STIMULATED LUMINESCENCE STUDIES IN ZINC-BASED FLUOROPERVOSKITES *Radiation Protection Dosimetry***179** 37–42

[18] Schwarz K and Blaha P 2003 Solid state calculations using WIEN2k *Computational Materials Science***28** 259–73

[19] Hohenberg P and Kohn W 1964 Inhomogeneous Electron Gas *Phys. Rev.***136** B864–71

[20] Kohn W and Sham L J 1965 Self-Consistent Equations Including Exchange and Correlation Effects *Phys. Rev.***140** A1133–8

[21] Perdew J P, Burke K and Ernzerhof M 1996 Generalized Gradient Approximation Made Simple *Phys. Rev. Lett.***77** 3865–8

[22] Monkhorst H J and Pack J D 1976 Special points for Brillouin-zone integrations *Phys. Rev. B***13** 5188–92

[23] Burriel R, Bartolome J, Gonzalez D, Navarro R, Ridou C, Rousseau M and Bulou A 1987 $KZnF_3$ cubic perovskite. Heat capacity and lattice dynamics *J. Phys. C: Solid State Phys.***20** 2819–27

[24] Poirier J P, Peyronneau J, Gesland J Y and Brebec G 1983 Viscosity and conductivity of the lower mantle; an experimental study on a MgSiO3 perovskite analogue, KZnF3 *Physics of the Earth and Planetary Interiors***32** 273–87

[25] Hofmeister A M 1991 Calculation of bulk modulus and its pressure derivatives from vibrational frequencies and mode Grüneisen Parameters: Solids with cubic symmetry or one nearest-neighbor distance *J. Geophys. Res.***96** 16181

[26] Hiadsi S, Bouafia H, Sahli B, Abidri B, Bouaza A and Akriche A 2016 Structural, mechanical, electronic and thermal properties of KZnF3 and AgZnF3 Perovskites: FP-(L)APW+lo calculations *Solid State Sciences***58** 1–13

[27] Jiang L Q, Guo J K, Liu H B, Zhu M, Zhou X, Wu P and Li C H 2006 Prediction of lattice constant in cubic perovskites *Journal of Physics and Chemistry of Solids***67** 1531–6

[28] Hadj Larbi A, Hiadsi S, Hadjab M and Saeed M A 2018 Optical study of cubic, and orthorhombic structures of XCaCl 3 (X = K, Rb) compounds: Comparative Ab initio calculations *Optik***166** 169–76

[29] Hadjab M, Guskova O, Bennacer H, Ziane M I, Larbi A H and Saeed M A 2022 Ground-state properties of p-type delafossite transparent conducting oxides 2H-CuMO2 (M=Al, Sc and Y): DFT calculations *Materials Today Communications***32** 103995

[30] Murnaghan F D 1944 The compressibility of media under extreme pressures *Proceedings of the National Academy of Sciences***30** 244–7

[31] Willardson R K, Weber E R, Paul W and Suski T 1998 *High pressure semiconductor physics I* (Academic Press)

[32] Born M 1940 On the stability of crystal lattices. I *Mathematical Proceedings of the Cambridge Philosophical Society***36** 160–72

[33] Mouhat F and Coudert F-X 2014 Necessary and sufficient elastic stability conditions in various crystal systems *Phys. Rev. B***90** 224104

[34] Ackland G J 2001 High-pressure phases of group IV and III-V semiconductors *Rep. Prog. Phys.***64** 483–516

[35] Grimvall G, Magyari-Köpe B, Ozoliņš V and Persson K A 2012 Lattice instabilities in metallic elements *Rev. Mod. Phys.***84** 945–86

[36] Wang J, Yip S, Phillpot S R and Wolf D 1993 Crystal instabilities at finite strain *Phys. Rev. Lett.***71** 4182–5

[37] Voight W 1928 Lehrbuch der kristallphysik *Teubner, Leipzig*

[38] Reuss A 1929 Computation of the yield point of mixed crystals due to hiring for single crystals *Math. Phys***9** 49–58

[39] Hill R 1952 The Elastic Behaviour of a Crystalline Aggregate *Proc. Phys. Soc. A***65** 349–54

[40] Wu Z, Zhao E, Xiang H, Hao X, Liu X and Meng J 2007 Crystal structures and elastic properties of superhard Ir N 2 and Ir N 3 from first principles *Phys. Rev. B***76** 054115

[41] Aguado F, Rodríguez F, Hirai S, Walsh J N, Lennie A and Redfern S A T 2008 High-pressure behaviour of KMF_3 perovskites *High Pressure Research***28** 539–44

[42] G V, V K, X Z, Y M, A S and NE C 2016 Calculated high-pressure structural properties, lattice dynamics and quasi particle band structures of perovskite fluorides KZnF 3 , CsCaF 3 and BaLiF 3 *J. Phys.: Condens. Matter***28** 315403

[43] Murtaza G, Khenata R, Khalid M N and Naeem S 2013 Elastic and optoelectronic properties of RbMF3 (M= Zn, Cd, Hg): A mBJ density functional calculation *Physica B: Condensed Matter***410** 131–6

[44] Pugh S F 1954 XCII. Relations between the elastic moduli and the plastic properties of polycrystalline pure metals *The London, Edinburgh, and Dublin Philosophical Magazine and Journal of Science***45** 823–43

[45] Greaves G N, Greer A L, Lakes R S and Rouxel T 2011 Poisson's ratio and modern materials *Nature Mater***10** 823–37

[46] Shah M A H, Nuruzzaman M, Hossain A, Jubair M and Zilani M A K 2023 A DFT insight into structural, mechanical, elasto-acoustic, and anisotropic properties of AePdH3 (Ae = Ca, Sr, Ba) perovskites under pressure *Computational Condensed Matter***34** e00774

[47] Frantsevich I N 1982 Elastic constants and elastic moduli of metals and insulators *Reference book*

[48] Haines J, Léger J and Bocquillon G 2001 Synthesis and Design of Superhard Materials *Annu. Rev. Mater. Res.***31** 1–23

[49] Fu H, Li D, Peng F, Gao T and Cheng X 2008 Ab initio calculations of elastic constants and thermodynamic properties of NiAl under high pressures *Computational Materials Science***44** 774–8

[50] Gaillac R, Pullumbi P and Coudert F-X 2016 ELATE: an open-source online application for analysis and visualization of elastic tensors *J. Phys.: Condens. Matter***28** 275201